THE JOURNAL OF BIOLOGICAL CHEMISTRY
Vol. 274, No. 31, Issue of July 30, pp. 21885–21892, 1999

Printed in U.S.A.

Structural Conservation of the Pores of Calcium-activated and Voltage-gated Potassium Channels Determined by a Sea Anemone Toxin*

(Received for publication, April 7, 1999)

Heiko Rauer‡, Michael Pennington§, Michael Cahalan‡, and K. George Chandy‡¶

From the ‡Department of Physiology and Biophysics, University of California, Irvine, California 92697 and §Bachem Bioscience Inc., King of Prussia, Pennsylvania 19406

The structurally defined sea anemone peptide toxins ShK and BgK potently block the intermediate conductance, Ca^{2+}-activated potassium channel *IKCa1*, a well recognized therapeutic target present in erythrocytes, human T-lymphocytes, and the colon. The well characterized voltage-gated *Kv1.3* channel in human T-lymphocytes is also blocked by both peptides, although ShK has a ~1,000-fold greater affinity for *Kv1.3* than *IKCa1*. To gain insight into the architecture of the toxin receptor in *IKCa1*, we used alanine-scanning in combination with mutant cycle analyses to map the ShK-*IKCa1* interface, and compared it with the ShK-*Kv1.3* interaction surface. ShK uses the same five core residues, all clustered around the critical Lys^{22}, to interact with *IKCa1* and *Kv1.3*, although it relies on a larger number of contacts to stabilize its weaker interactions with *IKCa1* than with *Kv1.3*. The toxin binds to *IKCa1* in a region corresponding to the external vestibule of *Kv1.3*, and the turret and outer pore of the structurally defined bacterial potassium channel, KcsA. Based on the NMR structure of ShK, we deduce the toxin receptor in *IKCa1* to have *x-y* dimensions of ~22 Å, a diameter of ~31 Å, and a depth of ~8 Å; we estimate that the ion selectivity lies ~13 Å below the outer lip of the toxin receptor. These dimensions are in good agreement with those of the KcsA channel determined from its crystal structure, and the inferred structure of *Kv1.3* based on mapping with scorpion toxins. Thus, these distantly related channels exhibit architectural similarities in the outer pore region. This information could facilitate development of specific and potent modulators of the therapeutically important *IKCa1* channel.

The intermediate conductance, calcium-activated potassium channel, *IKCa1*, plays a role in regulating membrane potential and in modulating the calcium signal in many different peripheral tissues (1–12), including human T-lymphocytes (3, 4), B-lymphocytes (EST accession no. AA937083), erythrocytes (AF042487, AF053403, AF072884), hemopoietic stem cells (AA558247), colonic epithelia (AA887697, T24528), pancreatic islets (AA076338, AA076337, AA122017), fibroblasts (AI034286), prostate (AA603035, AA65228), ovary (AA424836, AA443903, AA425636), testis (AI081834), and platelets (10). *IKCa1* is activated by intracellular calcium via a calmodulin-dependent mechanism (13), and its amino acid sequence exhibits ~40% identity with the sub-family of small conductance calcium-activated potassium channels (1–6). Clotrimazole, a potent but nonselective inhibitor of this channel, is currently being evaluated in the therapy of sickle cell disease and secretory diarrheas. Although initial results have been encouraging (5, 14–16), there is clearly a need for more specific inhibitors of *IKCa1*, and architectural information on this channel may facilitate drug development.

The use of peptide toxins to obtain insight into the topology of the external vestibule of potassium channels has a long and successful history. Structurally defined peptides from scorpion venom and sea anemone have been used as molecular yardsticks to gauge the dimensions and shape of the external vestibules of the voltage-gated *Shaker* and *Kv1.3* channels (17–23). The deduced dimensions are in good agreement with the recently published structure of the outer pore region of the bacterial potassium channel, KcsA, based on crystallographic data (24, 25). Therefore, the use of peptide toxins as mapping tools, set in the context of the known KcsA crystal structure, can facilitate the architectural mapping of the outer pore regions of pharmacologically important mammalian potassium channels in the absence of direct structural data for these channels.

Although *IKCa1* is only distantly related to the *Shaker* and *Kv1.3* voltage-gated channels, it is potently blocked by some of the same scorpion and sea anemone peptides that inhibit these channels. It might therefore be feasible to use the peptide-mapping approach to gain insight into the dimensions and shape of the toxin receptor on *IKCa1* and to compare this topology with the external vestibules of *Kv1.3* and *KcsA*. For this purpose, we have used the structurally defined 35-amino acid peptide toxin, ShK,[1] from the sea anemone *Stichodactyla helianthus*. We used the alanine scanning method, coupled with mutant cycle analyses, to map the interactive surface between ShK and *IKCa1* and compared this with the ShK:*Kv1.3* interface. Our studies indicate that ShK binds to *IKCa1* in an external vestibule that is architecturally similar to that of *Shaker*, *Kv1.3*, and *KcsA*, although ShK uses a significantly wider surface to interact with *IKCa1* compared with its interaction with *Kv1.3*. Such structural differences might be exploited to guide the design of novel peptides that specifically target *IKCa1*.

* This study was supported from funds from National Institutes of Health Grants MH59222 (to K. G. C.), NS14609 (to M. D. C.), GM54221 (to K. G. C. and M. P.), and by a fellowship from the Alexander von Humboldt Foundation (to H. R.). The costs of publication of this article were defrayed in part by the payment of page charges. This article must therefore be hereby marked "*advertisement*" in accordance with 18 U.S.C. Section 1734 solely to indicate this fact.

¶ To whom correspondence should be addressed: Dept. of Physiology and Biophysics, University of California Medical School, Joan Irvine Smith Hall, Rm. 291, Irvine, CA 92697. Tel.: 949-824-2133; Fax: 949-824-3143; E-mail: gchandy@uci.edu.

[1] The abbreviations used are: ShK, *Stichodactyla helianthus* toxin; BgK, *Bunodosoma granulifera* toxin; Dap, diaminopropionic acid; Nle, norleucine; Fmoc, *N*-(-9-fluorenyl)methoxycarbonyl.

MATERIALS AND METHODS

Peptide Synthesis—Fmoc-amino acid derivatives were obtained from Bachem A.G. (CH-4416 Bubendorf, Switzerland). Solid-phase assembly was initiated with an Fmoc-Cys(Trt)-2-chlorotrityl resin to minimize potential racemization of the C-terminal Cys residue. Automated stepwise assembly was carried out entirely on an ABI-431A peptide synthesizer (Applied Biosystems, Foster City, CA). The ShK analogues were solubilized, oxidized, and purified by reverse phase-high pressure liquid chromatography using the method described previously (23, 26), and high pressure liquid chromatography-pure fractions were pooled and lyophilized. The structure and purity of the peptides were confirmed by reverse phase-high pressure liquid chromatography, amino acid analysis, and electrospray ionization-mass spectroscopy analysis. Samples were weighed and adjusted to account for peptide content before bioassay.

Reagents—A cell line stably expressing *mKv1.3* (27) was maintained in Dulbecco's modified Eagle's medium containing 10% fetal calf serum and 1 mg/ml G418 (Life Technologies, Inc.). The *Kv1.3*-Val^{404} (His → Val) mutant has been described previously (20). The human *IKCa1* expression construct has previously been described (3, 4, 13), and the *IKCa1*-Lys^{239} mutant was a gift from Dr. J. Aiyar (Zeneca Pharmaceuticals, Wilmington, DE). The BgK peptide from *Bunodosoma granulifera* was a gift from Dr. A. Menez (Saclay, France).

Expression and Electrophysiological Analysis—The human wild-type *IKCa1* and *IKCa1*-Lys^{239} constructs were linearized with *Not*I, the *Kv1.3*-Val^{404} mutant with *Eco*RI, and these constructs were transcribed *in vitro* (20, 28). The cRNA along with a marker dye was injected into rat basophilic leukemia cells as described previously (13, 28). After 2–6 h, dye-containing cells with specific currents could be characterized using the patch-clamp method. Cell lines stably expressing *Kv1.3*-wild type (27) were trypsinized and plated onto glass coverslips at least 3 h before measurement. All cells were measured in the whole-cell configuration and bathed in mammalian Ringer solution with 0.1% bovine serum albumin (Sigma) containing (in mM): 160 NaCl, 4.5 KCl, 2 $CaCl_2$, 1 $MgCl_2$, 10 HEPES, adjusted to pH 7.4 with NaOH, with an osmolarity of 290–320 mOsm. In the K^+-Ringer solution, NaCl was replaced with KCl. A simple syringe-driven perfusion system was used to exchange the bath solutions in the recording chamber. The internal pipette solution for the *Kv1.3* channel recordings contained (in mM): 134 potassium fluoride, 1 $CaCl_2$, 2 $MgCl_2$, 10 HEPES, 10 EGTA, pH 7.2 (with KOH), 290–310 mOsm. The internal pipette solution for the *IKCa1* channel expressed in rat basophilic leukemia cells contained (in mM): 135 potassium aspartate, 2 $MgCl_2$, 10 HEPES, 10 EGTA, 8.7 $CaCl_2$, pH 7.2 (with KOH), 290–310 mOsm (free $[Ca^{2+}]_i$ = 1 μM). The holding potential in all experiments was −80 mV. *IKCa1* currents were activated with 1 μM internal Ca^{2+} and 200-ms voltage ramps from −150 to 50 mV applied every 5 s. *Kv1.3* currents were measured following 200-ms depolarizing pulses to 40 mV from the holding potential, applied every 30 s. Series resistance compensation (80%) was used if the current exceeded 2 nA. Capacitative and leak currents were subtracted using the P/8 procedure for *Kv1.3* currents. K_d values were calculated using the equation $K_d = ([\text{toxin}]/((1/y) - 1))$ with y = unblocked fraction; shown as mean ± S.D. where $n \geq 3$ for all experiments.

Free Energy Difference of Binding [ΔF]—The free energy difference of binding was calculated as $\Delta F = RT \ln(K_d \text{ ShK-analogue}/K_d \text{ ShK-wild type})$, where R = 1.987 cal/mol and T = 295° K (30). ΔF (in kcal mol^{-1}) is a measure of the difference in free energy between the interaction of an ShK analogue with the channel, compared with that of wild-type ShK (26).

Double Mutant Cycle Analysis—This method evaluates the strength of the interaction between any pair of channel and toxin residues. For each mutant cycle, we measured the potency (K_d) of ShK and its analogues on *IKCa1* and its mutants. The change in coupling energy, $\Delta\Delta G$, for a given pair of ShK-*IKCa1* residues and their mutants was calculated using the formula $\Delta\Delta G = kT \ln \Omega$, as described earlier (20, 23). Based on the studies of Schreiber and Fersht (29) and Hidalgo and MacKinnon (19), $\Delta\Delta G$ values ≥ 0.5 kcal mol^{-1} indicate that a particular pair of ShK and *IKCa1* residues are likely to lie within 5 Å of each other.

RESULTS

The Sea Anemone Toxins, ShK and BgK, Block IKCa1 and Kv1.3 Channels—We compared the toxin sensitivities of the two K^+ channels, present in activated human T lymphocytes, *IKCa1* and *Kv1.3*. Two potent peptide inhibitors, ShK and BgK, from the sea anemones *S. helianthus* and *B. granulifera*, were chosen for analysis (30, 31). These peptides share 31% sequence identity (Fig. 1*A*). Both contain six conserved cysteines that form three disulfide bonds, a feature common to many channel-blocking peptide inhibitors from scorpion venom as well as many defensins (32). However, the structures of ShK and BgK are significantly different from that of the scorpion toxins and defensins (23, 33, 34).

The cloned *IKCa1* and *Kv1.3* genes were expressed in mammalian cells, and representative currents are shown in Fig. 1*B*. *IKCa1* currents were elicited by 1 μM calcium in the pipette following break-in, whereas depolarizing pulses were used to generate *Kv1.3* currents. ShK and BgK, when applied externally, block the *IKCa1* channel in the low nanomolar range with K_d values of 30 ± 7 nM and 172 ± 43 nM, respectively (Fig. 1*B*, *left top panel*). BgK blocks *Kv1.3* with comparable potency (K_d = 39 ± 4 nM; Fig. 1*B*, *right top panel*). In contrast, ShK exhibits a markedly greater affinity for *Kv1.3* channels (K_d = 0.016 ± 0.003 nM) compared with *IKCa1* (Fig. 1*B*, *top panel*), indicating that this peptide has an exquisite ability to discriminate between the two T lymphocyte K^+ channels.

Determining the IKCa1 Channel-binding Surface of ShK—To elucidate the molecular basis for the ability of ShK to discriminate between *IKCa1* and *Kv1.3*, we used alanine-scanning mutagenesis to identify ShK residues essential for binding to both these channels. A series of monosubstituted peptide analogues, in which each residue is substituted with alanine, was tested for their ability to block the *IKCa1* and *Kv1.3* channels. The only exception is His^{19}, which was replaced by a lysine. Structurally critical ShK residues that were not substituted included the six half-cysteine residues, as well as Asp^5, Ala^{14}, and Gly^{33}. K_d values measured in this "Ala-scan" were used to calculate the free energy difference of binding, ΔF (see "Materials and Methods"). The greater the change in free energy (ΔF), the greater the influence of a particular ShK residue for channel binding.

In the representative example shown in Fig. 1*B* (*left*), an alanine substitution at ShK position 20 significantly reduces the affinity of the toxin for *IKCa1* (K_d = 2,450 nM) compared with that of the wild-type toxin (K_d = 30 nM). The change in free energy of binding, caused by this substitution, is 2.5 kcal mol^{-1}. Using this approach, we determined ΔF for each alanine substitution. The ShK residues most critical for *IKCa1* binding, with ΔF values greater than or equal to 2.5, are shown in *red* in Fig. 2*A* and include Arg^{11}, His^{19}, Ser^{20}, Lys^{22}, Tyr^{23}, Arg^{24}, and Phe^{27}. Alanine substitution at ShK position 21 (Met^{21}) also significantly disrupts the toxin-channel interaction (ΔF = 1.8; *orange*). Arg^1, Ile^7, Thr^{13}, Leu^{25}, and Ser^{26} (shown in *yellow*, where ΔF = 0.75–1.5), and Thr^6, Phe^{15}, Lys^{18}, and Arg^{29} (shown in *blue*, ΔF = 0.5–0.75), are only moderately important for binding, whereas Ala substitutions at the remaining ShK positions (shown in *white*, $\Delta F < 0.5$) have minimal effects (Fig. 2*A*).

Fig. 3 (*left*) shows the positions of the ShK residues (bottom and side view) that contribute to its interaction with *IKCa1*, color coordinated with the histograms in Fig. 2*A*. All the highly critical residues ($\Delta F \geq 2.5$) cluster together on one surface of the ShK peptide (*red*), and Met^{21} (*orange*) lies immediately adjacent. Residues with moderate influence (*yellow* and *blue*) form the margins of the ShK:*IKCa1*-binding surface. In general, nonessential residues cluster together on the opposite surface of the peptide (Fig. 3, *left*). Thus, the surface of ShK that binds *IKCa1* extends in its greatest distance from Arg^1 on one side to Phe^{15} on the other (Fig. 3, *left*, *bottom view*). Lys^{22} lies at the lowest point in the channel-binding surface (Fig. 3, *left*, *side view*).

Comparison of the ShK Toxin-binding Surfaces in IKCa1 and Kv1.3—All ShK analogues were tested on the *Kv1.3* channel to

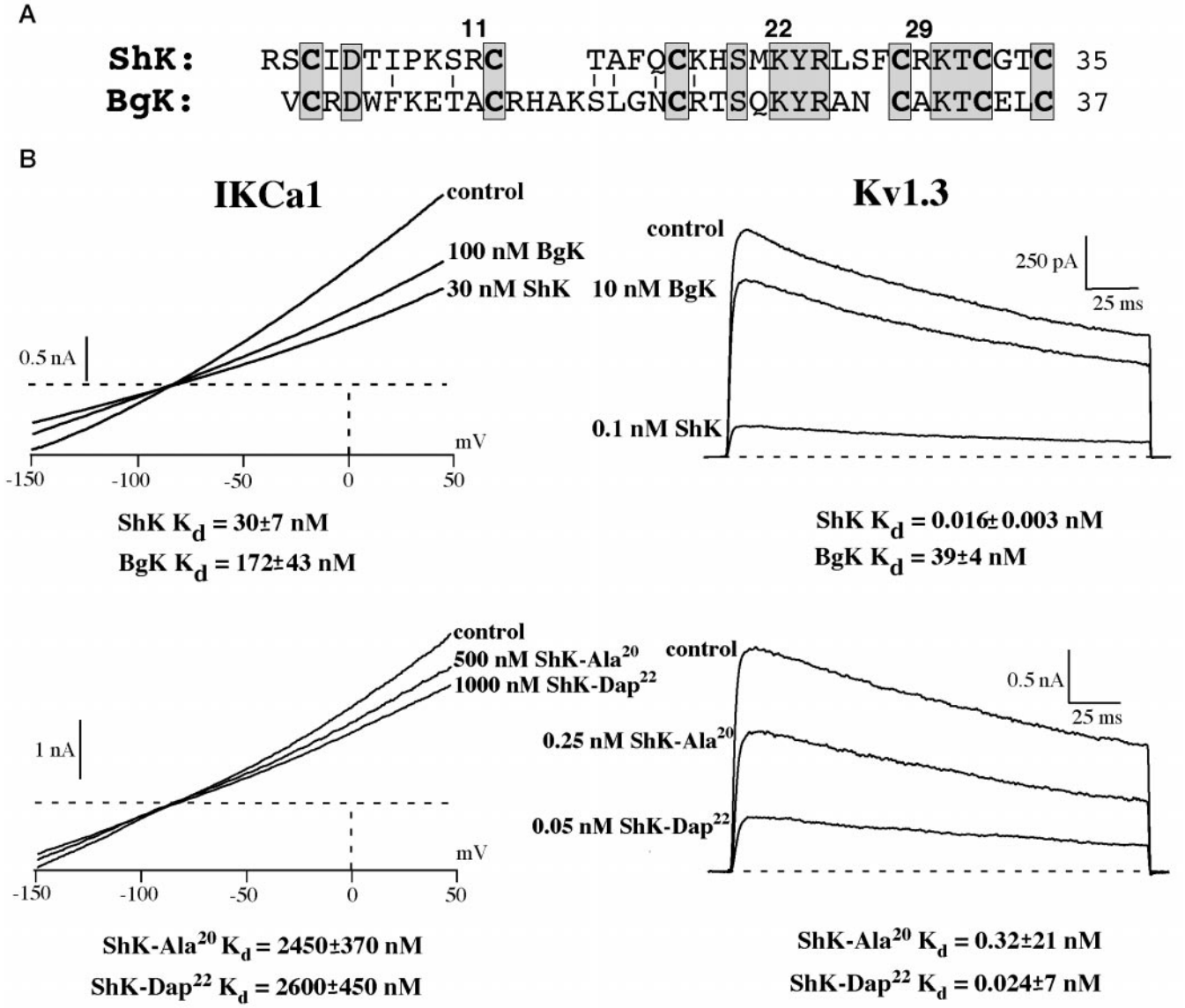

FIG. 1. **The sea anemone toxins, ShK and BgK, are potent inhibitors of *IKCa1* and *Kv1.3* channels.** *A,* alignment of the ShK and BgK amino acid sequence. Identical residues are *shaded*, conservative changes are connected with a line, the six conserved cysteines are shown in *bold*. *B,* IKCa1 and Kv1.3 currents in the presence and absence of ShK and BgK toxins. *Top panel*, wild-type ShK and BgK toxins block *IKCa1* (*left*) and *Kv1.3* (*right*) currents at low nanomolar to picomolar concentrations**.** *Bottom panel*, effect of two ShK analogues, ShK-Ala^{20} and ShK-Dap^{22}, on *IKCa1* (*left*) and *Kv1.3* (*right*) currents. The K_d-values for ShK, BgK, and the ShK analogues are indicated.

define the ShK-binding surface for this structurally well defined channel (20, 21, 23). Fig. 1*B*, *bottom panel*, compares the effect of one ShK alanine substitution (at ShK^{20}) on currents through *Kv1.3* and *IKCa1*, whereas Fig. 2*A* compares the ΔF values for all ShK substitutions on these channels. Replacements of His^{19}, Ser^{20}, Lys^{22}, Tyr^{23}, and Arg^{24} significantly disrupt the interaction of ShK with *Kv1.3* (ΔF values >1.5, *orange* and *red*), although to a lesser extent than with *IKCa1* ($\Delta F \geq 2.5$; Fig. 2*A*, and see Fig. 1*B*, *bottom panel*). Alanine substitutions at ShK positions 11, 21, and 27 ($\Delta F = 0.75$–1.5) and positions 1, 6, 7, 15, and 26 ($\Delta F < 0.75$) are also substantially less disruptive on *Kv1.3* compared with *IKCa1* (Fig. 2*B*). The only exception is ShK-Arg^{29}, which seems to be slightly more important for binding to *Kv1.3* than for *IKCa1* ($\Delta F = 0.88$ and 0.56, respectively). Our results thus suggest that ShK uses a larger number of residues to stabilize its interaction with *IKCa1* than with *Kv1.3,* although it uses the same core domain of five clustered residues for binding to both channels.

ShK-Lys^{22} protrudes into the *Kv1.3* pore and lies in close proximity to Tyr^{400} and Asp^{402} in the selectivity filter, and is critical for the interaction of the toxin with this channel (23). To determine the contribution of Lys^{22} to the interaction of the toxin with *IKCa1,* we compared the affinity of *IKCa1* and *Kv1.3* for four ShK-Lys^{22} analogues (Fig. 2*B*); we also examined the effect of these analogues on the *Kv1.3*-His$^{404} \rightarrow$ Val^{404} mutant, and these data are presented in a subsequent section. In two analogues, the positively charged lysine is replaced with the shorter, positively charged amino acids, ornithine (Orn) and diaminopropionic acid (Dap), whereas the other two analogues have the neutral residues norleucine (Nle) and alanine (Ala) at position 22. These residues differ in their side chain lengths (Dap, 2.5 Å; Ala, 2 Å; Orn, 5.0 Å; Nle, 5.0 Å; lysine, 6.3Å). Our results show that Ala^{22} and Nle^{22} substitutions significantly decrease the affinity of the toxin for both channels (Fig. 2*B*; $\Delta F \geq 2.1$), suggesting that the presence of these bulky neutral residues in the pore of either channel destabilizes the toxin-channel interaction. In contrast, the positively charged ShK-Dap^{22} and ShK-Orn^{22} exhibit different affinities for the two channels. The Dap^{22} substitution severely abrogates the affinity of the toxin for *IKCa1* ($\Delta F > 2.5$), but does not significantly

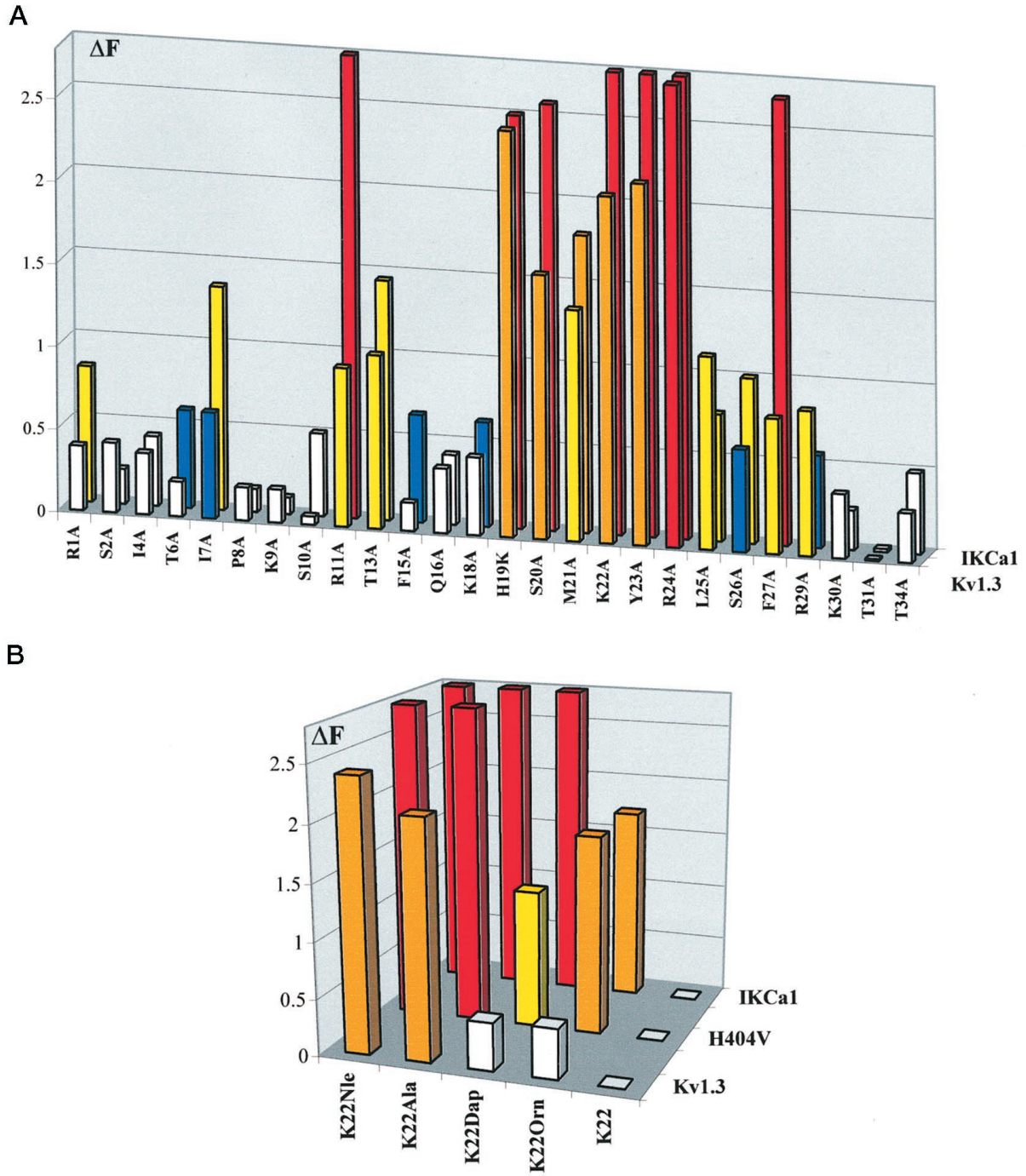

FIG. 2. **Free energy difference of binding (Δ*F*) due to specific substitutions in ShK.** *A,* ΔF values for ShK-Ala analogues on *IKCa1* and *Kv1.3*. Color code for Δ*F* values (in kcal mol^{-1}): *red,* Δ*F* ≥ 2.5 (values >2.8 are shown as 2.8); *orange*, Δ*F* = 1.5–2.5; *yellow*, Δ*F* = 0.75–1.5; *blue*, Δ*F* = 0.5–0.75; *white*, Δ*F* < 0.5. *B,* effect of ShK-Lys^{22} substitutions on binding to *Kv1.3, Kv1.3*-His^{404} → Val^{404} and *IKCa1* channels. Comparison of Δ*F* values for specific substitutions at ShK^{22} (color code as in *A*).

alter the affinity of ShK for *Kv1.3* (Fig. 1*B*, *bottom left* and Fig. 2*B*). The longer ShK-Orn^{22} substitution also significantly disrupts the affinity of the toxin for *IKCa1* (Δ*F* = 1.7), although to a lesser extent than Dap^{22}, possibly because it is better anchored in the channel pore, whereas this analogue blocks *Kv1.3* with potency equivalent to wild-type ShK (Fig. 2*B*).

Fig. 3 highlights the residues that ShK uses to interact with *IKCa1* (*left*) compared with those for *Kv1.3* (*right*). The residues are color-coordinated with the histogram in Fig. 2, *A* and *B*. ShK residues required for binding to both channels are clustered together on one surface (*colored*), whereas *white* residues not required for the interaction are located on the opposite toxin surface. ShK uses eight essential residues, Arg^{11}, His^{19}, Ser^{20}, Met^{21}, Lys^{22}, Tyr^{23}, Arg^{24}, and Phe^{27} to interact with *IKCa1*, whereas the toxin interaction with *Kv1.3* relies on only five essential contacts (His^{19}, Ser^{20}, Lys^{22}, Tyr^{23}, and Arg^{24}). Alanine substitutions at any of these five critical positions in the binding core domain severely disrupt the ShK-channel interaction in both channels (Δ*F* > 1.5, Fig. 3, *red* and *orange*). ShK residues that surround this critical core domain (ShK-positions 1, 6, 7, 11, 13, 15, 21, 26, and 27) exhibit a lower influence on binding to *Kv1.3* compared with *IKCa1*. Thus, the overall binding surface of ShK for *IKCa1* is larger and contains more essential interacting residues than its binding surface for

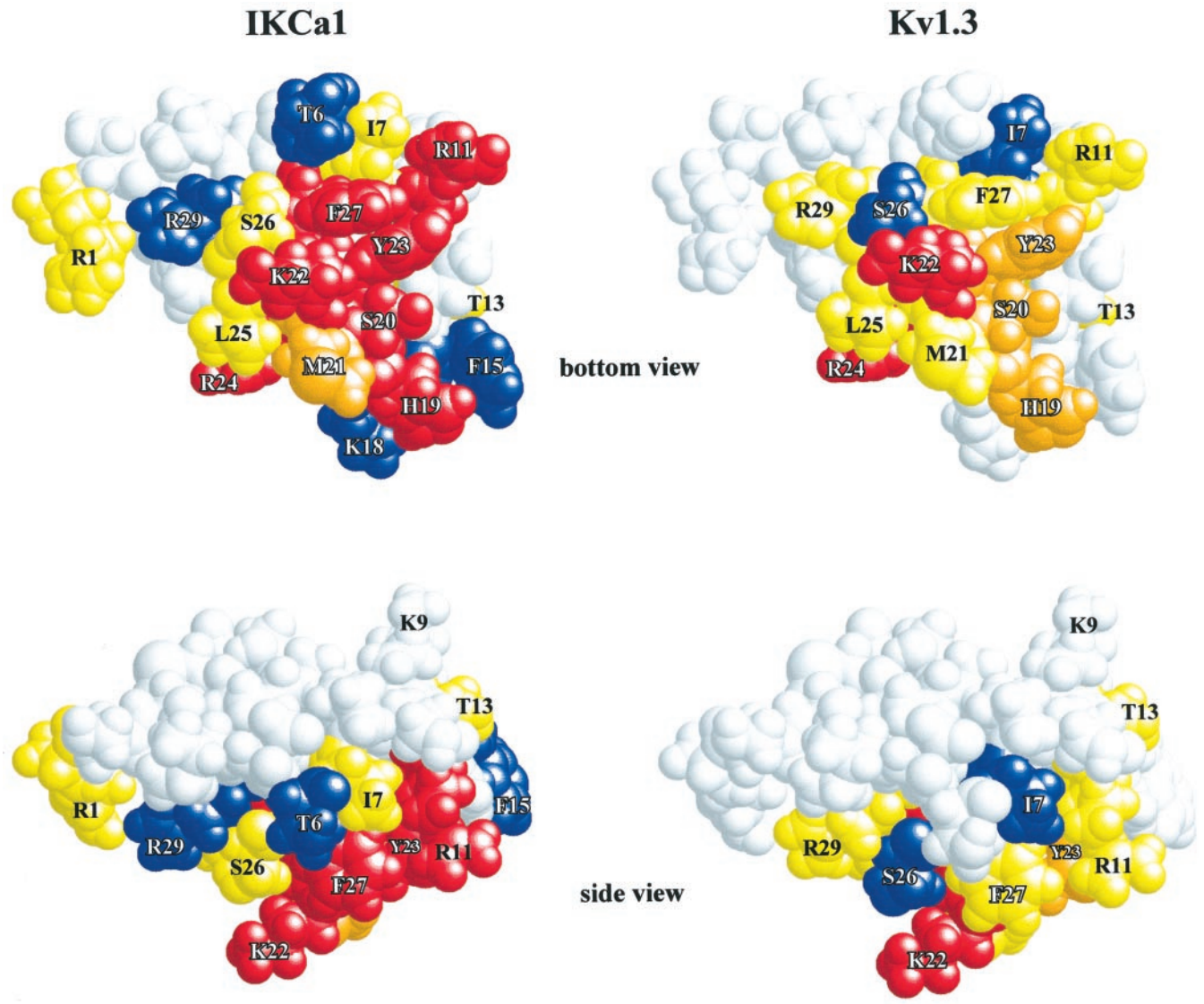

FIG. 3. **Channel-binding surface of ShK.** *Left panel,* surface of ShK that interacts with *IKCa1*; *right panel,* ShK surface that interacts with *Kv1.3.* ShK-binding surface is shown above (*bottom view*), and *side view* of the toxin is shown below. The residues are color coordinated to the histograms (ΔF values) in Fig. 2 (for color code, see Fig. 2*A*). The models were generated with the RasMol program.

Kv1.3 (Fig. 3). Nevertheless, the affinity of the toxin for *Kv1.3* is significantly greater than for *IKCa1* (Fig. 1*B*), suggesting that the picomolar affinity of ShK for *Kv1.3* is dependent on a few very tight toxin-channel contacts, whereas its ~1,000-fold lower nanomolar affinity for *IKCa1* is because of a greater number of weaker interactions.

Interactions of ShK with Residues in the External Vestibule of IKCa1—Peptides from scorpion and snake venom, as well as from sea anemone, bind to residues in the external vestibule of the ion conduction pathway of eukaryotic voltage-gated potassium channels and occlude their pores (17–23, 34). This vestibule corresponds to the outer pore and turret region in the structurally defined bacterial K^+ channel, KcsA (24), and mutations in the turret region of KcsA greatly enhance the ability of this channel to bind peptide inhibitors (25). We therefore undertook a series of mutational analyses to define the interactions of ShK with residues in the external vestibule of *IKCa1*.

Charge-reversal Mutation at IKCa1-Asp^{239} Dramatically Reduces Sensitivity to ShK—We first aligned the turret and pore regions of *KcsA, Kv1.3*, and *IKCa1* (Fig. 4*A*). All three channels are remarkably similar in the pore region with absolute conservation of the GYGD motif (Fig. 4*A*). Interestingly, *IKCa1* contains an aspartate (Asp^{239}) at the position homologous to Asp^{386} in the turret of *Kv1.3* that is essential for the interaction of *Kv1.3* with ShK and various scorpion toxins (20, 23). A charge-reversal mutation involving Asp^{386} in *Kv1.3* (Asp → Lys) substantially reduces the channel sensitivity to ShK ($\Delta F = 1.9$), kaliotoxin ($\Delta F > 2.5$), and charybdotoxin ($\Delta F > 2.5$) (20, 23). The converse charge-reversal mutation at the homologous position in KcsA (Arg^{64} → Asp^{64}) enhances this channels sensitivity for agitoxin-2 (25). We therefore replaced *IKCa1* Asp^{239} with the positively charged Lys, and examined the sensitivity of the mutant channel to ShK. The *IKCa1*-Lys^{239} mutant was expressed in rat basophilic leukemia cells, and representative currents, elicited by 1 μM calcium in the pipette solution, are shown in Fig. 4*B*. The mutant channel is ~18-fold less sensitive to ShK (K_d = 548 ± 37 nM) than wild-type *IKCa1*, suggesting that the Asp → Lys charge-reversal mutation at position 239 in *IKCa1* has the same consequences on ShK binding as the identical mutation at the homologous position in *Kv1.3* (23). The change in free energy for this channel mutant (ΔF = 1.7 kcal mol^{-1}) is equivalent to severe Ala substitutions (ΔF >1.5 kcal mol^{-1}) in ShK (compare with Fig. 2*A*), indicating

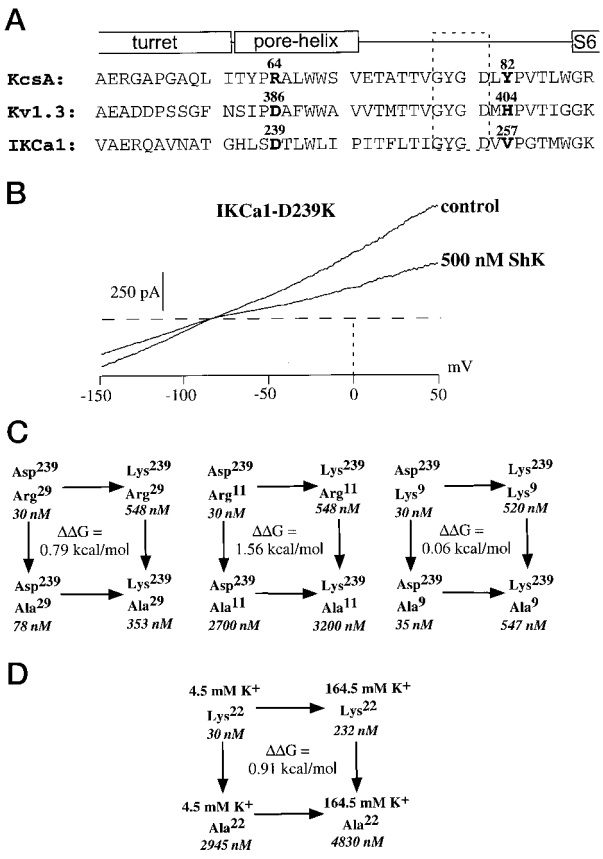

FIG. 4. **ShK binds in the external vestibule of *IKCa1*.** *A,* amino acid sequence alignment of the turret and pore region of KcsA, Kv1.3, and IKCa1. *Kv1.3* residues critical for toxin binding (Asp^{386}, His^{404}) and the corresponding residues in *KcsA* (Arg^{64}, Tyr^{82}) and *IKCa1* (Asp^{239}, Val^{257}) are highlighted. The selectivity filter motif (GYGD) is conserved (*dotted line*). *B, IKCa1*-Lys^{239} currents in the absence or presence of ShK. Typical *IKCa1*-Lys^{239} currents are about half-blocked by 500 nM ShK (K_d = 548 ± 37 nM). *C,* mutant cycles of *IKCa1*-Asp^{239} with ShK-Arg^{11}, ShK-Arg^{29}, and ShK-Lys^{9}. The differences in free coupling energy, $\Delta\Delta G$, show strong coupling between *IKCa1*-Asp^{239} and Shk-Arg^{29} and ShK-Arg^{11}, whereas ShK-Lys^{9} is not coupled. *D,* mutant cycle showing proximity of ShK-Lys^{22} to a potassium-binding site in the channel pore. Mutant cycle with ShK and ShK-Ala^{22} on *IKCa1* using external solutions with 4.5 and 164.5 mM K^+ showed a strong coupling ($\Delta\Delta G$ = 0.91 kcal mol^{-1}) of ShK-Lys^{22} to a potassium-binding site in the selectivity filter of the *IKCa1* pore.

that this channel residue is a critical contact point at the toxin-channel interface.

IKCa1-Asp^{239} Interacts with ShK-Arg^{11} and ShK-Arg-,sup>29—Asp^{386} in *Kv1.3* and the corresponding Arg^{64} in KcsA are positioned at the periphery of the base of the external vestibule, and Asp^{239} might therefore be expected to occupy an equivalent position in *IKCa1*. Because ShK-Arg^{29} interacts with Asp^{386} in *Kv1.3* (23), we used mutant cycle analysis to determine whether this peptide residue is close to Asp^{239} in *IKCa1*. Two additional ShK residues were evaluated for their ability to interact with Asp^{239}. ShK-Arg^{11} is ~21 Å from Arg^{29} on the channel-binding surface, whereas ShK-Lys^{9} is on the nonbinding surface of ShK (Fig. 3). Fig. 4*C* shows the three mutant cycles that were used to analyze the ShK interactions with *IKCa1*-Asp^{239}. ShK-Arg^{29} and ShK-Arg^{11} couple tightly with *IKCa1*-Asp^{239} ($\Delta\Delta G$ values = 0.79 and 1.56 kcal mol^{-1}, respectively), suggesting that these toxin residues are within ~5 Å of Asp^{239} in different *IKCa1* subunits, Arg^{11} being closer to Asp^{239} than Arg^{29}. As expected, because of its position on the opposite site of the interactive toxin surface, ShK-Lys^{9} does not couple with *IKCa1*-Asp^{239} ($\Delta\Delta G$ = 0.06 kcal mol^{-1}). Because Arg^{11} and Arg^{29} lie ~21 Å apart and are oriented at an angle of ~105° from the center of the toxin, they most likely interact with Asp^{239} residues in adjacent subunits (Fig. 5, *left*), as has been reported for *Kv1.3* (23) rather than with Asp^{239} in opposite *IKCa1* subunits.

ShK-Lys^{22} Protrudes into the IKCa1 Pore and This Interaction Is Dependent on the K^+ Ion Concentration in the Pore—Because Lys^{22} is located at the lowest and central point in the channel-binding surface of ShK (Fig. 3), there is a good likelihood that it lies close to or within the pore of *IKCa1*, as has been reported for *Kv1.3* (23). To test this idea, we examined whether the terminal amine of ShK-Lys^{22} lies close to a potassium-binding site in the ion selectively filter. Earlier studies have shown that Lys^{22} in ShK, and the homologous Lys^{27} in the scorpion toxins, agitoxin-2 and kaliotoxin, lie in close proximity to a potassium-binding site in the ion selectivity filter of the *Kv1.3* and *Shaker* channels (21, 22). Occupancy of this site by a K^+ ion appears to destabilize the interaction of the native toxins with these channels via electrostatic repulsion of Lys^{27}, because it has little effect on toxin analogues containing neutral substitutions at position 27 (21, 22). Similarly, potassium ions were shown to inhibit the interaction between Lys^{27} (but not Asn^{27}) in charybdotoxin and residues in the pore of the large conductance, calcium-activated K^+ channel, BK (35). We have used a similar approach to determine whether ShK-Lys^{22} lies in the vicinity of a potassium-binding site in the *IKCa1* pore. We compared the effect of changing the external K^+ concentration from 4.5 to 164.5 mM on the affinity of the *IKCa1* channel for ShK-Lys^{22} and ShK-Ala^{22}. Consistent with earlier reports, increasing external [K^+] also reduces the potency of ShK-Lys^{22} on the *IKCa1* channel (7.7-fold), whereas block by ShK-Ala^{22} is minimally affected (1.6-fold). We assessed the strength of this interaction using mutant cycle analysis (Fig. 4*D*). The $\Delta\Delta G$ value for this cycle (0.91 kcal mol^{-1}) indicates that ShK-Lys^{22} lies within 5 Å of a K^+-binding site located in the *IKCa1* pore, as has been reported for *Kv1*.3 (23).

Since ShK-Lys^{22} protrudes into the pores of both *IKCa1* and *Kv1.3*, why is the *IKCa1* pore more sensitive to ShK-Lys^{22} substitutions than the *Kv1.3* pore, especially those involving shorter positive charged residues (Orn^{22} and Dap^{22})? A comparison of the sequences of the outer pore regions of the two channels suggests an explanation (Fig. 4*A*). *Kv1.3* contains a histidine (His^{404}) at the entrance to its pore that is positioned just above the selectivity filter, whereas *IKCa1* contains a hydrophobic residue (Val^{257}) at the corresponding position. Might the difference in the nature of the residue at the pore entrance account for the differential sensitivity to Shk-Dap^{22} and Shk-Orn^{22}? To test this possibility, we replaced *Kv1.3*-His^{404} with valine, a mutation that makes the outer pore of *Kv1.3* more closely resemble that of *IKCa1*, and tested the sensitivity of this channel to the ShK^{22} analogues. In keeping with our hypothesis, the *Kv1.3*-Val^{404} mutant behaves more like *IKCa1* with respect to all ShK-Lys^{22} substitutions (Fig. 2*B*). We were unable to determine the effect of the reverse mutation (Val^{257} → His) on the sensitivity of *IKCa1* to the Lys^{22} analogues, because this channel mutant is nonfunctional. These results are consistent with the notion that the differential responsiveness of the *Kv1.3* and *IKCa1* pores to ShK^{22} substitutions is due, in part, to the residue at the channel mouth of *Kv1.3* (His^{404}) and the homologous position in *IKCa1*. In summary, ShK binds residues in the external vestibule of *IKCa1*, with ShK-Arg^{11} and Arg^{29} interacting with Asp^{239} residues in adjacent subunits of *IKCa1* and with ShK-Lys^{22} projecting into the pore.

DISCUSSION

Using alanine-scanning mutagenesis, we have compared the surface that ShK, a 35-amino acid peptide toxin from the sea

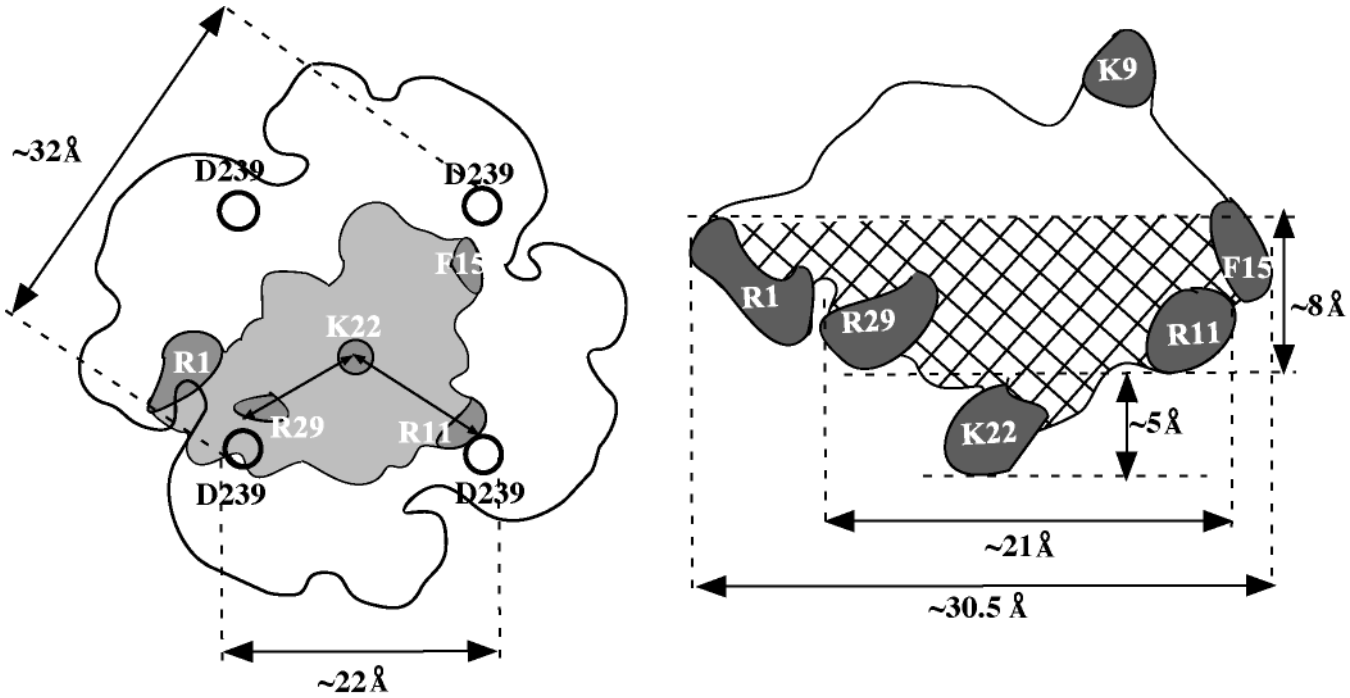

FIG. 5. **Topology of the ShK-binding site.** Dimensions of the external vestibule of *IKCa1* were determined using the NMR-derived ShK structure as a molecular caliper. *Left,* schematic representation of the external vestibule with Asp^{239} residues highlighted (derived from the KcsA structure) with ShK (*gray*) docked. ShK-Arg^{11} and Arg^{29} are ~21 Å apart, interacting with Asp^{239} residues in adjacent channel subunits. ShK-Lys^{22} is shown at the geometric center of the tetramer, protruding into the pore. In this geometry Arg^1 and Phe^{15} (at opposing ends of the ShK:*IKCa1*-binding surface) are located at opposite channel subunits. The diameter of the tetramer based on the distance between ShK-Arg^1 to Phe^{15} and the Asp^{239} *x-y* triangulation is approximately 31 Å. *Right,* schematic side view of the ShK toxin (compare Fig. 3, *bottom*) with the channel-binding surface highlighted. The distances between key toxin residues are indicated and correspond approximately to dimensions of the *IKCa1* external vestibule (see "Discussion").

anemone *S. helianthus,* uses to interact with two distinct potassium channels present in activated human T-lymphocytes: the intermediate conductance, Ca^{2+}-activated K^+ channel *IKCa1*, and the voltage-gated K^+ channel *Kv1.3*. Although using the same core domain, the *IKCa1*-binding surface of ShK is more extensive than its *Kv1.3*-binding surface, and yet ShK blocks *Kv1.3* with ~1,000-fold greater potency than *IKCa1*. A few tight *Kv1.3*-ShK contacts appear to underlie the picomolar affinity of ShK for *Kv1.3*, whereas the *IKCa1*-ShK interface is stabilized by a greater number of weaker interactions.

Because ShK interacts with *IKCa1* and *Kv1.3* using the same core domain involving His^{19}, Ser^{20}, Lys^{22}, Tyr^{23}, and Arg^{24} (Fig. 3), this toxin is likely to sit in both channels with a similar geometry. Several lines of evidence support this idea. First, charge-reversal mutations at homologous positions in *IKCa1* ($Asp^{239} \rightarrow Lys^{239}$) and *Kv1.3* ($Asp^{386} \rightarrow Lys^{386}$) reduce the sensitivity of these channels to ShK block in a similar fashion. Second, ShK-Arg^{29} shows energetic coupling with Asp^{239} in *IKCa1*, as well as with the homologous *Kv1.3*-Asp^{386} (Fig. 4*C*) (23). Third, ShK-Arg^{11} and ShK-Arg^{29} appear to couple with residues in adjacent subunits of *IKCa1* as has been reported for *Kv1.3* (23). Fourth, the critical ShK-Lys^{22} lies close to a potassium-binding site in the selectivity filter of the *Kv1.3* pore (23), and mutant cycle analyses suggests the same is true for *IKCa1* (Fig. 4*D*). Last, replacement of the critical ShK-Lys^{22} with bulky neutral residues (Nle and Ala) substantially reduces the affinity of the toxin for both channels, possibly because such residues are not tolerated in the channel pore. These results indicate that ShK binds to *IKCa1* in a region corresponding to the external vestibules of *Kv1.3* and uses a comparable docking geometry. Such a docking configuration would place Arg^1 and Phe^{15}, the two residues at opposite margins of the *IKCa1*-binding surface (Fig. 3*A*), in close proximity to channel residues in opposite subunits in the *IKCa1* tetramer (Fig. 5).

Knowing the NMR structure of ShK (33) and its approximate docking configuration in *IKCa1*, we used this peptide as a structural template to estimate the dimensions of the toxin receptor in the external vestibule of *IKCa1*. We have obtained two independent estimates of the diameter of the toxin receptor in the *IKCa1* external vestibule. First, we estimate the width of the *IKCa1* toxin receptor to be ~31 Å (Fig. 5) based on the width of the *IKCa1*-binding surface of ShK (distance from Arg^1 to Phe^{15}). Second, the *x-y* dimension of the toxin receptor is estimated to be ~22 Å (Fig. 5, *left*), based on the distance between the two toxin residues, ShK-Arg^{11} and ShK-Arg^{29} (Fig. 5, *right*), that interact with Asp^{239} residues in adjacent *IKCa1* subunits. This value implies (by Pythagorean triangulation) a distance of ~31 Å between Asp^{239} residues in opposite subunits (Fig. 5). We estimate that the toxin receptor is approximately ~8–9 Å deep, based on the vertical distance between one horizontal line joining Arg^1 and Phe^{15}, and a second horizontal line connecting the terminal amines of Arg^{11} and Arg^{29} (Fig. 5, *right*). The selectivity filter is estimated to lie ~12–13 Å below the outer edge of the toxin receptor in the vestibule based on the vertical distance between the terminal amine of Lys^{22} and the horizontal line joining Arg^1 and Phe^{15} (Fig. 5, *right*). Our deduced dimensions of the toxin receptor in the *IKCa1* vestibule are in good agreement with those obtained by crystallography for the KcsA vestibule (24, 25), and by toxin-mapping for *Kv1.3* (20, 21, 23) and *Shaker* (17–19, 22).

Thus, the *IKCa1* external vestibule appears to be topologically similar to those of the distantly related *Kv1.3, Shaker*, and *KcsA* channels, a result that provides support for the development of homology models of the *IKCa1* outer pore based on the KcsA crystal structure. The experimentally determined differences in the ShK-*IKCa1* and ShK-*Kv1.3* binding interfaces raises the possibility of designing novel peptides and small molecule inhibitors that selectively target the *IKCa1*

channel. Such reagents might be useful in elucidating the role of the *IKCa1* channel in diverse cell types and may also have therapeutic value.

Acknowledgments—We appreciate the expert technical assistance of Luette Forrest and Annabelle Chia-ling Wu, as well as valuable discussions with George A. Gutman, Stephan Grissmer, Ray Norton, and William Kem. We thank Dr. A. Menez (Saclay, France) for the kind gift of BgK and Dr. J. Aiyar (Zeneca Pharmaceuticals, Wilmington, DE) for the *hIKCa1*-Lys^{239} construct.

REFERENCES

1. Joiner, W. J., Wang, L. Y., Tang, M. D., and Kaczmarek, L. K. (1997) *Proc. Natl. Acad. Sci. U. S. A.* **94,** 11013–11018
2. Ishii, T. M., Silvia, C., Hirschberg, B., Bond, C. T., Adelman J. P., and Maylie, J. (1997) *Proc. Natl. Acad. Sci. U. S. A.* **94,** 11651–11656
3. Logsdon, N. J., Kang, J., Togo, J. A., Christian, E. P., and Aiyar, J. (1997) *J. Biol. Chem.* **272,** 32723–32726
4. Ghanshani, S., Coleman, M., Gustavsson, P., Wu, C.-L., Gutman, G. A., Dahl, N., Mohrenweiser, H., and Chandy, K. G. (1998) *Genomics* **51,** 160–161
5. Vandorpe, D. H., Shmukler, B. E., Jiang, L., Lim, B., Maylie, J., Adelman, J. P., de Franceschi, L., Cappellini, M. D., Brugnara, C., and Alper, S. L. (1998) *J. Biol. Chem.* **273,** 21542–21553
6. Jensen, B. S., Stroebaek, D., Christophersen, P., Joergensen, D. T., Hansen, C., Silahtaroglu, A., Olesen, S.-P., and Ahring, P. K. (1998) *Am. J. Physiol.* **275,** C848–C856
7. Gardos, G. (1958) *Biochim. Biophys. Acta* **30,** 653–654
8. Brugnara, C., Armsby, C. C., De Franceschi, L., Crest, M., Euclaire, M. F., and Alper, S. L. (1995) *J. Membr. Biol.* **147,** 71–82
9. Grissmer, S., Nguyen, A. N., and Cahalan, M. D. (1993) *J. Gen. Physiol.* **102,** 601–630
10. Mahaut-Smith, M. P. (1995) *J. Physiol.* **484,** 15–24
11. Cahalan, M. D., and Chandy, K. G. (1997) *Curr. Opin. Biotechnol.* **8,** 749–756
12. Verheugen, J. A. H. (1998) *J. Physiol.* **508,** 167–177
13. Fanger, C. M., Ghanshani, S., Logsdon, N. J., Rauer, H., Kalman, K., Zhou, J., Beckingham, K., Chandy, K. G., Cahalan, M. D., and Aiyar, J. (1999) *J. Biol. Chem.* **274,** 5746–5754
14. Rufo, P. A., Jiang, L., Moe, S. J., Brugnara, C., Alper, S. L., and Lencer, W. I. (1996) *J. Clin. Invest.* **98,** 2066–2075
15. Brugnara, C., Gee, B., Armsby, C. C., Kurth, S., Sakamoto, M., Rifai, N., Alper, S. L., and Platt, O. S. (1996) *J. Clin. Invest.* **97,** 1227–1234
16. Rufo, P. A., Merlin, D., Riegler, M., Ferguson-Maltzman, M. H., Dickinson, B. L., Brugnara, C., Alper, S. L., and Lencer, W. I. (1997) *J. Clin. Invest.* **100,** 3111–3120
17. Stocker, M., and Miller, C. (1994) *Proc. Natl. Acad. Sci. U. S. A.* **91,** 9509–9513
18. Goldstein, S. A., Pheasant, D. J., and Miller, C. (1994) *Neuron* **12,** 1377–1388
19. Hidalgo, P., and MacKinnon, R. (1995) *Science* **268,** 307–310
20. Aiyar, J., Withka, J. M., Rizzi, J. P., Singleton, D. H., Andrews, G. C., Lin, W., Boyd, J., Hanson, D., Simon, M., Dethlefs, B., Lee, C.-L., Hall, J. E., Gutman, G. A., and Chandy, K. G. (1995) *Neuron* **15,** 1169–1181
21. Aiyar, J., Rizzi, J. P., Gutman, G. A., and Chandy, K. G. (1996) *J. Biol. Chem.* **271,** 31013–31016
22. Ranganathan, R., Lewis, J. H., and MacKinnon, R. (1996) *Neuron* **16,** 131–139
23. Kalman, K., Pennington, M., Lanigan, M. D., Nguyen, A., Rauer, H., Mahnir, V., Paschetto, K., Kem, R., Grissmer, S., Gutman, G. A., Christian, E. P., Cahalan, M. D., Norton, R. S., and Chandy, K. G. (1998) *J. Biol. Chem.* **273,** 32697–32707
24. Doyle, D. A., Cabral, J. M., Pfuetzner, R. A., Kuo, A., Gulbis, J. M., Cohen, S. L., Chait, B. T., and MacKinnon, R. (1998) *Science* **280,** 69–77
25. MacKinnon, R., Cohen, S. L., Kuo, A., Lee, A., and Chait, B. T. (1998) *Science* **280,** 106–109
26. Pennington, M. W., Mahnir, V. M., Khaytin, I., Zaydenberg, I., Byrnes, M. E., and Kem, W. R. (1996) *Biochemistry* **35,** 16407–16411
27. Grissmer, S., Nguyen, A., Aiyar, J., Hanson, D., Mather, R. J., Gutman, G. A., Karmilowicz, M. J., Auperin, D. D., and Chandy, K. G. (1994) *Mol. Pharm.* **45,** 1227–1234
28. Rauer, H., and Grissmer, S. (1996) *Mol. Pharmacol.* **50,** 1625–1634
29. Schreiber, G., and Fersht, A. R. (1995) *J. Mol. Biol.* **248,** 478–486
30. Castaneda, O., Sotolongo, V., Amor, A. M., Stocklin, R., Anderson, A. J., Harvey, A. L., Engstrom, A., Wernstedt, C., and Karlsson, E. (1995) *Toxicon* **33,** 603–613
31. Aneiros, A., Garcia, I., Martinez, J. R., Harvey, A. L., Anderson, A. J., Marshall, D. L., Engstrom, A., Hellman, U., and Karlsson, E. (1993) *Biochim. Biophys. Acta* **1157,** 86–92
32. Bontems, F., Roumestand C., Gilquin B., Menez, A., and Toma, F. (1991) *Science* **254,** 1521–1523
33. Tudor, J. E., Pallaghy, P. K., Pennington, M., and Norton, R. S. (1996) *Nat. Struct. Biol.* **3,** 317–320
34. Dauplais, M., Leqoc, A., Song, J., Cotton, J., Jamin, N., Gilquin, B., Roumestand, C., Vita, C., de Medeiros, C. L. C., Rowan, E. G., Harvey, A. L., and Menez, A. (1997) *J. Biol. Chem.* **272,** 4302–4309
35. Naini, A. A., Shimony, E., Kozlowski, E., Shaikh, T., Dang, W., and Miller, C. (1996) *Neuropharmacology* **35,** 915–921